Catalysis Science & Technology

PAPER

View Article Online
View Journal | View Issue

Cite this: *Catal. Sci. Technol.*, 2019, **9**, 5456

Study on the catalytic performance of different crystal morphologies of HZSM-5 zeolites for the production of biodiesel: a strategy to increase catalyst effectiveness†

Elyssa G. Fawaz,[a] Darine A. Salam, *[a] L. Pinard[b] and T. Jean Daou [cd]

Strategies to improve molecular transport and accessibility of ZSM-5 zeolites were investigated for the model reaction of esterification of linoleic acid with methanol for biodiesel production. Zeolite crystals with a short diffusion length and hierarchical porosity were compared with conventional coffin-shaped microcrystals for their catalytic activity in terms of acidic properties and pore structure. As-synthesized catalytic materials were fully characterized with XRD, SEM, TEM, N_2 adsorption–desorption, X-ray fluorescence, and FTIR. The results showed that hierarchical zeolites with nanosheet and nanosponge morphologies achieved the highest catalytic performance due to improved accessibility and mass transfer of linoleic acid from the outer mesoporous surface to the intrinsic active zeolitic framework. A maximum conversion of 95.12% was reached for the esterification of linoleic acid using HZSM-5 nanosheets at 4 h reaction time, 10 wt% catalyst loading, 6 : 1 methanol to linoleic acid molar ratio and 180 °C. Despite the high conversions achieved with HZSM-5 nanosponges (86.40% (SD = 1.77)), these catalysts did not operate to their full acidic potential as compared to HZSM-5 nanosheets, due to their higher hydrophilicity which hindered linoleic acid adsorption onto their surface. HZSM-5 nanosheets' regenerability was tested under optimum reaction conditions and showed a high methyl ester conversion for 4 consecutive cycles.

Received 18th July 2019,
Accepted 22nd August 2019

DOI: 10.1039/c9cy01427f

rsc.li/catalysis

1. Introduction

Biodiesel produced from waste renewable resources is a non-toxic, environmentally friendly and biodegradable alternative fuel to the depleted diesel of petroleum origins.[1,2] Conventionally, biodiesel is produced by a transesterification reaction using a homogeneous base catalyst.[3] Despite being cheap, readily available and having high catalytic efficiency, this procedure is exceedingly sensitive to water and free fatty acid (FFA) contents in the oil-feedstock. At high contents, the saponification reaction occurs and creates several drawbacks in subsequent recovery and purification of methyl esters due to the difficult separation of products and the increase in viscosity.[4,5] Freedman *et al.* stated that homogeneous acid catalysts are unresponsive to FFA content and are superior to base catalysts in the transesterification of an oil-feedstock containing more than 1% FFAs.[6] However, this process also presents different drawbacks such a lengthy reaction time, which might be surmounted by heterogeneous acid catalysts. These solid catalysts minimize the complications related to homogeneous catalysis in terms of segregation, recovery and regeneration of the catalyst.[7,8] Further, transesterification of oils using solid acid catalysts is non-corrosive and eliminates the extensive product purification step.[9,10] Nonetheless, the development of three phases (alcohol, oil and solid catalyst) remains a main problem connected to heterogeneous catalyst usage in transesterification reactions, as it lowers the biodiesel yield and the rate of the reaction by restraining the diffusion of reagents and products.[11,12] Zeolites are crystal-like solids having a precise framework of oxygen, aluminum and silicon in their structure.[13] They have found applications in several aspects of catalysis,[14–17] especially in esterification reactions for biodiesel production.[18–23] They show high acid activity and a large total surface area with shape selective characteristics that are non-existent in comparable amorphous catalysts.[24–27] However, they are usually produced in

[a] *Department of Civil and Environmental Engineering, Maroun Semaan Faculty of Engineering and Architecture, American University of Beirut, P.O. Box: 11-0236, Riad El Solh, Beirut, Lebanon. E-mail: ds40@aub.edu.lb; Fax: +961(1)744 462; Tel: +961(1)350 000, Ext. 3609*

[b] *Institut de Chimie des Milieux et Matériaux de Poitiers, UMR 7285 CNRS, 86073 Poitiers Cedex 9, France*

[c] *Université de Haute Alsace, Axe Matériaux à Porosité Contrôlée (MPC), Institut de Science des Matériaux de Mulhouse (IS2M), UMR CNRS 7361, ENSCMu, 68093 Mulhouse, France*

[d] *Université de Strasbourg, Strasbourg, France*

† Electronic supplementary information (ESI) available. See DOI: 10.1039/c9cy01427f

micropores, with micrometer-range crystal dimensions and so, with an insignificant external surface area. These characteristics limit the conversion of bulky molecules. Alternative strategies enhancing mass transfer in zeolite-catalyzed reactions by shortening the diffusion length to the nanometer range and introducing hierarchical porosity (micro- and mesoporosities) could make the active sites in the zeolites more accessible and thus the heterogeneous acid esterification involving large molecules such as fatty acids more feasible. Aside from possessing a high specific surface area and notable porosity which can increase the contact between the solid catalyst and the oil molecules, hierarchical ZSM-5 was found to be a promising catalyst in esterification reactions. For instance, mesoporous zeolite ZSM-5 crystals have been successfully fabricated by Jin *et al.*[28] The synthesized mesoporous ZSM-5 showed improved catalytic performance compared with conventional ZSM-5 in reactions such as esterification reactions. Nandiwale *et al.* (2015) synthesized a hierarchical H-ZSM-5 catalyst for the esterification of acetic acid with benzyl alcohol.[29] The hierarchical HZSM-5 was found to be a promising catalyst for benzylation with a conversion of 94% which was obtained at a reaction temperature of 70 °C after 2 h. To the best of our knowledge, only one study tested the esterification of oleic acid with ethanol for biodiesel production using microporous ZSM-5 and beta and micro/mesoporous ZSM-5 acid zeolites to assess how the internal mass transfer limitation is affected by the zeolite's pore size. However, despite exhibiting better internal mass transfer, ZSM-5 zeolites showed the lowest catalytic activity.[30] In the current study, the catalytic behavior of ZSM-5 zeolites exhibiting distinct crystal morphologies (conventional coffin-shaped microcrystals, nanocrystals, nanosheets, and nanosponges) was assessed in terms of acidic properties and pore structure in the esterification of linoleic acid, as a model biodiesel production reaction. The influencing factors of esterification including the molar ratio of methanol to linoleic acid, reaction temperature and reaction time were analyzed. The Thiele modulus model was used to discuss the correlation between effective mass transfer within the pore size of the zeolites and their catalytic performance based on experimental results.

2. Experimental section

Tetrapropylammonium hydroxide was used as a template for conventional zeolites, whereas bifunctional compounds which could engender micropores and mesopores simultaneously were specifically synthesized to produce hierarchical ZSM-5.

2.1. Structure directing agent synthesis

The di-quaternary ammonium-type structure directing agent (SDA) $C_{22}H_{45}$-$N^+(CH_3)_2$-C_6H_{12}-$N^+(CH_3)_2$-$C_6H_{13}Br_2$ (abbreviated as C22-6-6), used for ZSM-5 nanosheet synthesis, was synthesized following a modified procedure reported by Na *et al.*[31] For the production of ZSM-5 nanosponges, the zeolite-SDA-functional surfactant $C_{18}H_{37}$-$N^+(CH_3)_2$-C_6H_{12}-$N^+(CH_3)_2$-C_6H_{12}-$N^+(CH_3)_2$-$C_{18}H_{37}(Br^-)_3$ (abbreviated as 18-N_3-18) was prepared as described in ref. 32. Detailed synthesis description of C22-6-6 and 18-N_3-18 is provided in the ESI† (section S1).

For all reactions, the solvent used in the preparation of the SDAs was evaporated at room temperature for product precipitation. Products were further filtered, washed with diethyl ether, and dried in a vacuum oven for 2 h, at 50 °C.

The purity of the solid organic products C22-6-6 and 18-N_3-18 was checked by solution-state ^{1}H NMR, with $CDCl_3$ as the solvent.

2.2. Catalyst synthesis

Typical ZSM-5 zeolite big crystals (MC) with coffin-shape morphologies were synthesized by dissolving 0.26 g of sulfuric acid (Aldrich) and 3.19 g of tetraethoxysilane (TEOS, Aldrich, 98%) in 10.75 g of distilled water in a 45 ml stainless steel ®Teflon-lined autoclave. 0.36 g of sodium hydroxide (Riedel de Haen, 99%) and 0.1 g of $Al_2(SO_4)_3{\cdot}18H_2O$ (Rectapur, 99%) were added to the mixture. 3.03 g of tetrapropylammonium hydroxide (TPAOH) aqueous solution (25 wt%, Fluka) was finally supplemented to meet the gel's molar composition of $100SiO_2 : 1Al_2O_3 : 30Na_2O : 18H_2SO_4 : 20TPAOH : 4000H_2O$.[33] The gel was then stirred at 1000 rpm for 30 min, heated at 60 °C for 4 hours and finally deposited in a tumbling oven for 4 days, at 30 rpm and 150 °C.

ZSM-5 zeolite nanocrystals (NC) were synthesized following the molar composition $50SiO_2 : 1C_9H_{21}O_3Al : 6NaBr : 10TPAOH : 450H_2O$. 0.31 g of $C_9H_{21}O_3Al$ and 12.1 g of tetrapropylammonium hydroxide (25 wt% TPAOH aqueous solution, Fluka) were dissolved in 3 g of distilled water and stirred for 20 min at room temperature. 0.93 g of NaBr was added to the solution which was stirred for 20 additional minutes. 4.48 g of porous silica gel (100 mesh) was then added and well mixed with the solution. The gel was finally placed in an oven at 170 °C for 24 hours.

The synthesis of ZSM-5 nanosheets (NSh) followed the same procedure described for ZSM-5 zeolite large crystals with coffin-shape morphology, with the only difference being the usage of 1.08 g of the di-quaternary ammonium-type surfactant (C22-6-6) instead of tetrapropylammonium hydroxide aqueous solution (25 wt%). The composition of the gel was therefore $100SiO_2 : 1Al_2O_3 : 30Na_2O : 18$C22-6-6 $: 4000H_2O$.

To produce ZSM-5 nanosponges (NS), a molar composition of $100SiO_2 : 2.5Al_2O_3 : 22Na_2O : 800EtOH : 5$ 18-N_3-18 $: 7100H_2O$ was adopted as described by Na *et al.*[32] Accordingly, 0.08 g of sodium aluminate ($NaAlO_2$ with 56.7 wt% Al_2O_3, 39.5 wt% Na_2O, and 3.3 wt% H_2O), 0.26g of sodium hydroxide (Riedel de Haen, 99%), 3.54 g of tetraethoxysilane (TEOS, Aldrich, 98%), 3.07 g of EtOH (99%), and 1.28 g of 18-N_3-18 were dissolved in distilled water under stirring in a ®Teflon-lined stainless steel autoclave. The gel was stirred at 1000 rpm at room temperature for 30 min, then at 60 °C for 6 hours and finally placed in a tumbling oven for 5 days at 30 rpm and 150 °C.

After synthesis, the different ZSM-5 zeolites were filtered, washed with distilled water, dried overnight at 105 °C, and finally calcined at 550 °C for 8 h in air to remove the organic structuring agents.

An ion exchange process using NH_4Cl as a precursor was used to modify the synthesized Na-ZSM-5 zeolites. Dried zeolites were added to a 1 M solution of NH_4Cl with a ratio of 1 : 20 and heated under stirring at 80 °C for 2 h in a round bottom flask fitted with a reflux condenser. The ion exchange process was repeated three times and the mixture was recurrently washed with distilled water, dried at 105 °C and then calcined in air for 10 h at 550 °C to obtain the H^+ exchanged-zeolite ready for catalysis. The exchanged zeolites of HZSM-5 big crystals, nanocrystals, nanosheets and nanosponges were labeled MC-HZSM-5, NC-HZSM-5, NSh-HZSM-5, and NS-HZSM-5, respectively.

2.3. Catalyst characterization

A PANalytical MPD X'Pert Pro diffractometer equipped with an X'Celerator real-time multi-strip detector (2.122° 2θ active length) and operating with Cu Kα radiation (λ = 0.15418 nm) was used to obtain the X-ray diffraction patterns and purity of the produced zeolite materials. The zeolite's diffractogram was recorded at 22 °C in the low range $0.5 < 2\theta < 5°$ and wide range $3 < 2\theta < 50°$ (220 s time step and 0.017° 2θ angle step).

The homogeneity and morphology of the produced crystals were examined using a 7 kV accelerating voltage scanning electron microscope (SEM) (Philips XL 30 FEG microscope) and a transmission electron microscope (TEM) (Philips model CM200), working with a 0.3 nm point-to-point resolution, at 200 kV.

The surface area, micropore size and micropore volume of the produced zeolites were determined by N_2 sorption (ASAP 2420 system, Micromeritics, USA) and calculated adopting the BET method using areas of $2 \times 10^{-4} < p/p_0 \leq 8 \times 10^{-2}$ and $4 \times 10^{-3} < p/p_0 \leq 12 \times 10^{-2}$ for the microcrystals (MC-HZSM-5) and nanocrystalline materials (nanosheets (NSh-HZSM-5), nanosponges (NS-HZSM-5), and nanocrystals (NC-HZSM-5)), respectively. The micropore volumes (V_{micro}) were calculated using the *t*-plot method and the pore size distribution was determined by using the Barrett–Joyner–Halenda (BJH) model applied on the desorption branch. The total pore volume was calculated at p/p_0 = 0.9 and the mesopore volume was determined by subtracting the micropore volume from the total volume. Prior to single measurements, 50 mg of the zeolite samples was outgassed for 15 h, at 300 °C. Measurements of nitrogen sorption were carried out at −196 °C.

X-ray fluorescence spectroscopy (Philips, Magic X) was used to determine the Si/Al molar ratio of the produced samples and to evaluate their successful exchange.

Pyridine adsorption followed by infrared spectrometry in a Thermo Nicolet Magna 550-FT-IR spectrometer was used to measure the amount of Lewis and Brønsted acid sites. Samples of zeolite were squeezed into self-supported pellets of 20 mg. Each wafer was then preheated at 450 °C in an analysis cell for 12 h, in air. The cell was later placed under vacuum for 1 h to remove physisorbed molecules after decreasing the wafer temperature to 200 °C. Prior to introducing pyridine into the cell for 5 min, the temperature was further reduced to 150 °C. The cell was then evacuated to 10^{-6} bar and after 1 h of vacuum, the IR spectra were recorded at room temperature. The amounts of Brønsted [$PyrH^+$] and Lewis [PyrL] acid sites were established using extinction coefficients previously determined in ref. 34, following integration of peak areas at 1545 cm^{-1} and 1454 cm^{-1}, respectively.

^{27}Al (I = 5/2) magic angle spinning (MAS) NMR was carried out with a Bruker Avance II 400 spectrometer operating at B_0 = 9.4 T (Larmor frequency ν_0 = 104.2 MHz) equipped with a Bruker 2.5 mm double channel probe. The rotor was spun at 25 kHz, and free induction decays (FID) were collected with a $p/12$ rf pulse (0.6 ms) and a recycle delay of 1 s. Measurements were carried out with $[Al(H_2O)_6]^{3+}$ as an external standard reference.[14] The decomposition of the spectra was performed using the DMFit software[35] in order to determine the Si/Al ratio of the framework (coupled with XRF results).

2.4. Esterification reactions

For all types of HZSM-5 produced, esterification reactions of linoleic acid (ACROS, 99%) with methanol (Chromasolv, 99.9%) were performed by refluxing in a 50 ml round-bottom reactor, under stirring (550 rpm). The reactor was loaded with 0.6 ml (equivalent to 0.54 g or 1 mole) of linoleic acid and the desired amount of methanol (6 : 1, 12 : 1 or 25 : 1 methanol to linoleic acid by molar ratio) was next supplemented. For each methanol to oil ratio, esterification reactions were performed at three different temperatures (60, 140 and 180 °C) at a catalyst loading of 10 wt% for 6 h. The catalyst was dried prior to reaction at 105 °C. Kinetic studies were performed for the HZSM-5 type which showed the highest conversions under a defined set of reaction conditions. For the conditions used, the esterification reactions were carried out over 24 h by sacrificing triplicate samples at predetermined time intervals (0, 0.5, 1, 2, 3, 4, 8, 16, and 24). Blank experiments were also performed in triplicate for each parameter varied.

At the end of the esterification reactions, the content of the reaction flasks was extracted with 50 ml of methanol to dissolve the water produced during the esterification reaction, followed by two dichloromethane (DCM) (Fisher, 99.8%) extractions of 50 mL each to dissolve the residual linoleic acid and produced methyl esters. The liquid extracts were separated from the solid catalysts by gravity filtration through a bed of filtration beads and 0.2 μm filter paper and analyzed for methyl esters and residual linoleic acid.

2.5. Fatty acid and methyl ester analysis

Gas chromatography (GC) analysis (Trace GC Ultra, Thermo Scientific) was used to obtain the methyl ester content in the liquid extracts. The GC was equipped with an HP-INNOWAX capillary column (30 m × 250 μm × 0.25 μm) and a flame

ionization detector (FID). The FID was set at 300 °C, the injector temperature was 250 °C in splitless mode, and the injection volume of the sample was 5 μl. Helium was used as a carrier gas at 1 mL min^{-1}. After the isothermal period (2 min at 60 °C), the temperature of the oven was increased from 60 °C to 200 °C at a 10 °C min^{-1} heating rate, and lastly increased to 240 °C at a 5 °C min^{-1} ramp and maintained for 7 min. Peaks of methyl esters were identified based on reference standards (Supelco 37 component FAME mix in DCM, TraceCert). Eqn (1) was used to determine the conversion of linoleic acid in the esterification reaction:

$$\text{Conversion}(\%) = \frac{\sum C_{\text{methyl esters}} \times V_{\text{extract}}}{M_{0\ \text{Linoleic acid}}} \times 100 \quad (1)$$

where $C_{\text{methyl esters}}$ is the concentration in mg L^{-1} quantified by GC/FID, V_{extract} is the total volume (L) of the liquid extract, and $M_{0\ \text{Linoleic acid}}$ is the initial mass of linoleic acid in mg added to the reactor.

Residual linoleic acid was analyzed with a high-performance liquid chromatograph (HPLC) equipped with a UV visible diode array detector (Agilent Technologies, CA, USA), using the method described by Gratzfeld-Husgen and Schuster.[36] Bromophenacyl bromide (Fluka, Buchs SG, Switzerland) was used to obtain the corresponding esters of FAs after derivatization. A C8 column (150 × 2.1 mm ZORBAX Eclipse XDB, 5 μm) was used. The sample injection volume was 1 μL, and the detection wavelength for the esters of FAs was 258 nm. The mobile phase was composed of a mixture of water (A) and acetonitrile + 1% tetrahydrofuran (B) and a solvent gradient of 30% B at 0 min, 70% B at 15 min, and 98% B at 25 min was used.

2.6. Determination of the kinetics of the esterification reaction

Eqn (2) describes the stoichiometric relationship of the reactants and products of the esterification reaction.

$$\text{Linoleic acid} + \text{Methanol} \xrightarrow{\text{Catalyst}} \text{Methyl linoleate} + H_2O \quad (2)$$

According to the general equation (eqn (2)), the reaction rate can be obtained as follows (eqn (3)):

$$-r_a = -\frac{1}{S}\frac{dC_{LA}}{dt} = k' \cdot C_{LA} \cdot C_{Me} \quad (3)$$

where r_a is the reaction rate (mg L^{-1} m^2 h^{-1}), C_{LA} is the linoleic acid concentration (mg L^{-1}), C_{Me} is the methanol concentration (mg L^{-1}), S is the surface area of the solid catalyst, and k' is the reaction rate constant (mg^{-1} L m^2 h^{-1}).

The amount of linoleic acid (LA) molecules adsorbed is equal to the sum of the amount desorbed and the amount of linoleic acid consumed by the chemical reaction on the surface and intrisically.[37] According to the following assumptions, the reaction rate (1) is described as:

$$-r_a = -\frac{1}{S}\frac{dC_{LA}}{dt} = k_s' \theta_M C_{LA,s} \cdot C_{Me,s} \quad (4)$$

where C_{LA} is the oleic acid concentration in the bulk liquid phase, k_s' is the chemical reaction constant on the catalyst surface, θ_M is the occupied fraction of active sites by methanol, and $C_{LA,s}$ is the concentration of linoleic acid on the catalyst surface.

Corresponding to the suggested reaction mechanism, the adsorption of LA is the rate-limiting step. Then the net rate of LA adsorption–desorption is equal to the reaction rate on the catalyst surface (5):

$$r_{ads-des} = k_{ads}\left(1 - \sum\theta\right)C_{LA} - k_{des}C_{LA,s} = -r_{LA} = -\frac{1}{S}\frac{dC_{LA}}{dt} = k_s C_{LA,s} \quad (5)$$

where $r_{ads-des}$ is the net rate of LA adsorption–desorption, k_{ads} and k_{des} are the respective adsorption and desorption rate constants, and $\sum\theta$ is the total solid fraction covered by all species in the liquid mixture.

Eqn (5) can be reorganized to get the non-measurable $C_{LA,s}$ with respect to the measurable C_{LA} (6):

$$C_{LA,s} = \frac{k_{ads}\left(1 - \sum\theta\right)}{k_{des} + k_s\theta_M} C_{LA} \quad (6)$$

Substitution of eqn (6) into eqn (4) results in eqn (7):

$$-r_a = -\frac{1}{S}\frac{dC_{LA}}{dt} = \left(k_s\theta_M\right)\frac{k_{ads}\left(1 - \sum\theta\right)}{k_{des} + k_s\theta_M} C_{LA} C_{Me} \quad (7)$$

All reactions can be viewed as a result of two consecutive steps. The first is the meeting of two reactant molecules by diffusion. The second is the reaction step, in which the reactants conquer an activation barrier and a diffusion limitation. The esterification reaction in the presence of a zeolite catalyst is reaction-controlled. As a result, the observed rate coefficient is only relevant to the reaction step and is equal to the intrinsic rate coefficient.[38] As discussed above, assuming that the adsorbed reaction components governed by the net rate of LA adsorption–desorption contribute to the intrinsic reaction, the intrinsic rate coefficient (k_{eff}) would be (8):

$$k_{eff} = \left(k_s\theta_M\right)\frac{k_{ads}\left(1 - \sum\theta\right)}{k_{des} + k_s\theta_M} \quad (8)$$

Eqn (4) thus becomes:

$$-r_a = -\frac{1}{S}\frac{dC_{LA}}{dt} = k_{eff} C_{LA} C_{Me} \quad (9)$$

where k_{eff} (mg^{-1} L m^2 h^{-1}) reflects both the chemical reaction and adsorption–desorption resistance on the surface.

Equation (9) follows a second order reaction rate. Nevertheless, methanol's concentration throughout the heterogeneous reaction could be considered constant due to the

excess methanol added to push the reaction in the direction of product formation. Consequently, the concentration of methanol does not modify the order of the reaction which will behave as a first order reaction and obey pseudo-first order kinetics (eqn (10)).[39,40]

$$-r_a = -\frac{1}{S}\frac{dC_{LA}}{dt} = k_{eff}\cdot C_{LA}\cdot C_{Me} = k\cdot C_{LA} \quad (10)$$

where k ($m^2\ h^{-1}$) = $k_{eff}C_{Me} \approx cst$, when methanol is used in excess.

Assuming that the initial concentration of linoleic acid is $C_{0\ LA}$ at time $t = 0$ and becomes $C_{t\ LA}$ at time t, the integration of eqn (10) from $t = 0$ to $t = t$, and $C_{0\ LA}$ to $C_{t\ LA}$ gives eqn (11):

$$\ln C_{0\ LA} - \ln C_{t\ LA} = k\cdot t \quad (11)$$

From the mass balance of the reaction,

$$X_{ME} = 1 - \frac{C_{tLA}}{C_{0LA}}$$

where X_{ME} is the methyl ester yield. Upon rearrangement of eqn (11), the kinetics of linoleic acid conversion could be expressed as follows (12):

$$\ln(1 - X_{ME}) = -k\cdot t \quad (12)$$

3. Results and discussion

3.1. Catalyst characterization

3.1.1. XRD. As illustrated in Fig. 1a and b, only the MFI-type zeolite crystalline phase was attained for all the zeolites, which confirms the high purity achieved for the different morphologies of ZSM-5. However, hierarchical zeolites (NSh-HZSM-5 and NS-HZSM-5) display wider and less intense XRD peaks compared to NC-HZSM-5 and MC-HZSM-5 samples, as already suggested by Kabalan *et al.*[41] The use of C22-6-6 and C18-N_3-C18 as structure directing agents for NSh-ZSM-5 and NS-ZSM-5, respectively, produced nanosheets and nanosponges with meso-structuration recognized by the presence of broad peaks at low diffraction angles ($0.6° < 2\theta < 5°$) as shown in Fig. 1c. The broad peaks of NSh-ZSM-5 at low

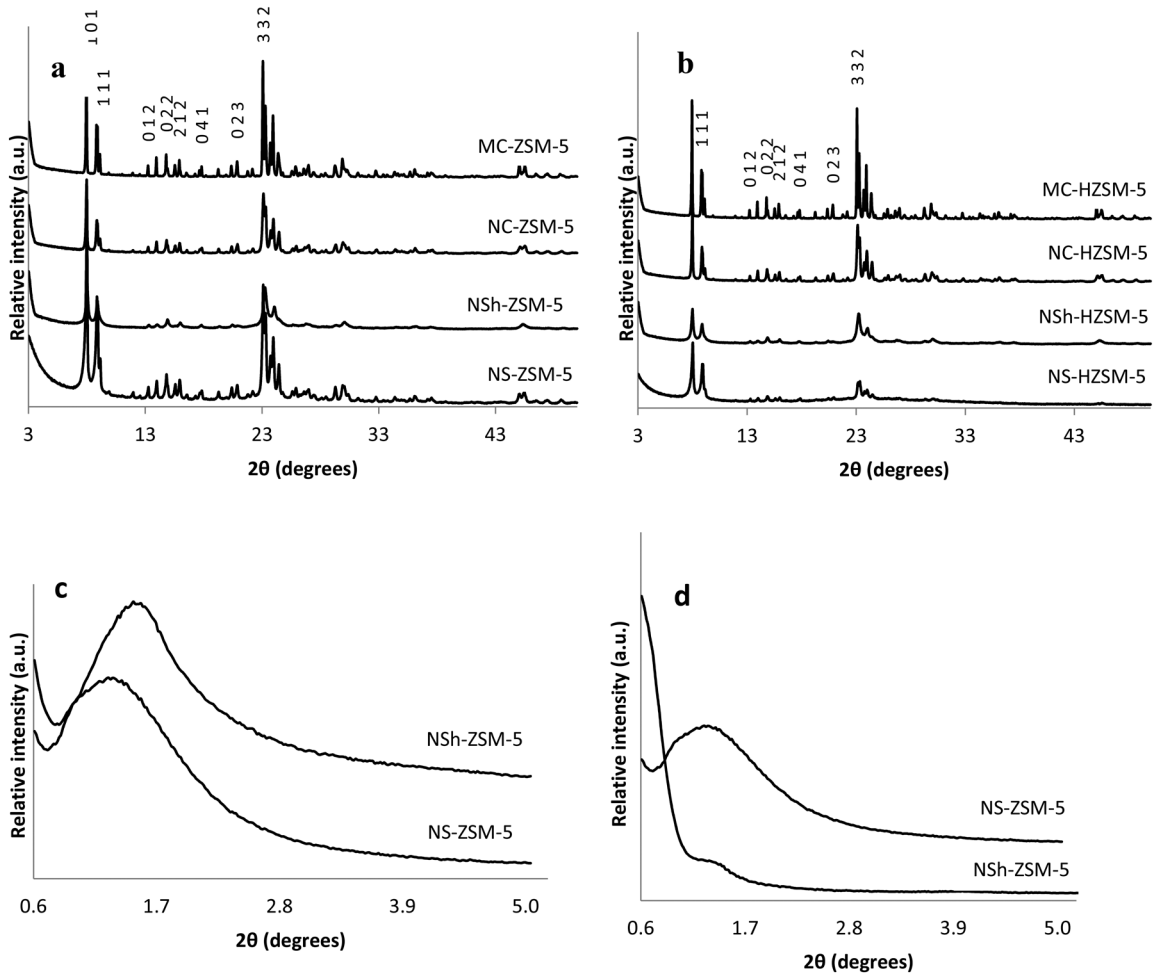

Fig. 1 (a) Wide angle XRD patterns of calcined MC-ZSM-5, NC-ZSM-5, NSh-ZSM-5, and NS-ZSM-5, (b) wide angle XRD patterns of exchanged and calcined MC-HZSM-5, NC-HZSM-5, NSh-HZSM-5, and NS-HZSM-5, (c) low angle patterns of non-calcined NSh-ZSM-5 and NS-ZSM-5, and (d) low angle patterns of calcined NSh-ZSM-5 and NS-ZSM-5.

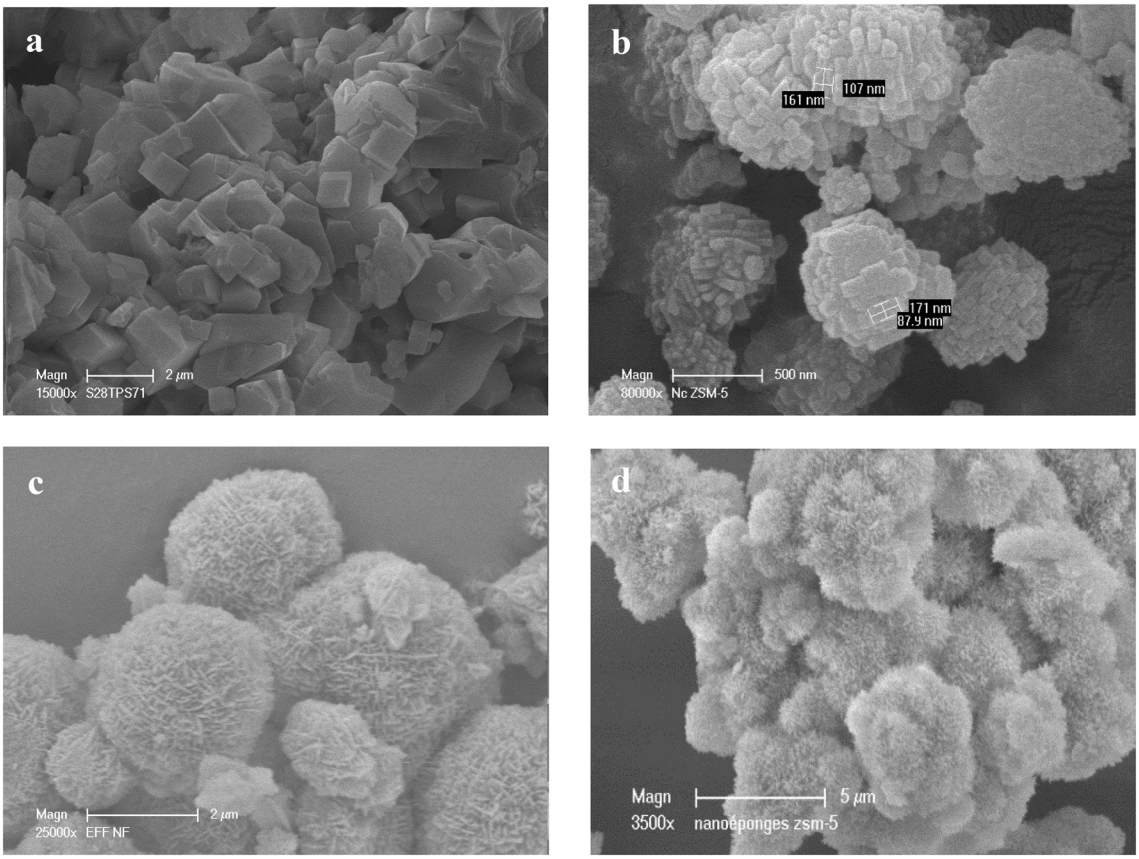

Fig. 2 Scanning electron microscopy (SEM) images of (a) MC-HZSM-5, (b) NC-HZSM-5, (c) NSh-HZSM-5, and (d) NS-HZSM-5.

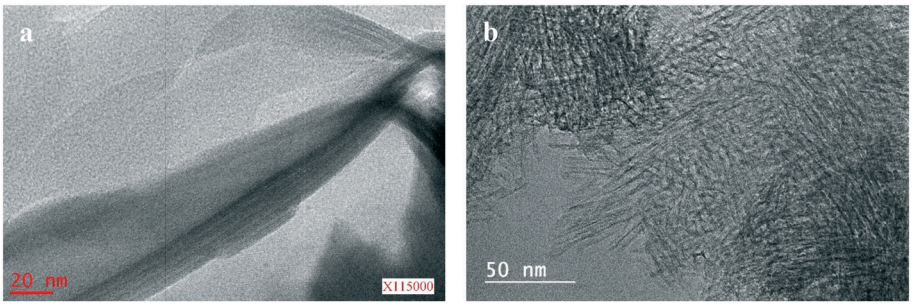

Fig. 3 Transmission electron microscopy (TEM) images of (a) NSh-HZSM-5 and (b) NS-HZSM-5.

diffraction angles disappear after calcination, indicating that the organization of materials on the mesoscopic scale is due to the presence of C22-6-6 which acts as a structure and shape directing agent. Meanwhile, the XRD peak at low angles remains intact for NS-ZSM-5 after calcination (Fig. 1d). This suggests that the calcined nanosponge samples have a higher mesopore volume which was later confirmed by N_2 sorption tests. At wide angles, only the diffraction peaks relative to the (*h*0*l*) crystallographic planes are strong enough to be properly indexed for NSh-HZSM-5. This indicates that the hydrophobic alkyl tail of C22-6-6 blocked the crystal growth along the *b*-crystal axis, and that the zeolite layers are amassed in multilamellar arrays confirming thus nanosheet formations.[31] The XRD pattern of NS-HZSM-5 suggests a 2D hexagonal symmetry of micropores stacked in two different orientations.[32]

3.1.2. SEM and TEM. The SEM images displayed in Fig. 2 show the different morphologies observed for the HZSM-5 synthesized zeolites. Micrometric crystals with parallelepiped shape were obtained for MC-HZSM-5, with crystal sizes ranging between 3.4 and 7 μm (Fig. 2a). NC-HZSM-5 showed particles with an average size of 500 nm to 1000 nm composed of agglomerated crystals having an average size of 85 to 310 nm (Fig. 2b). The replacement of TPAOH by the bifunctional

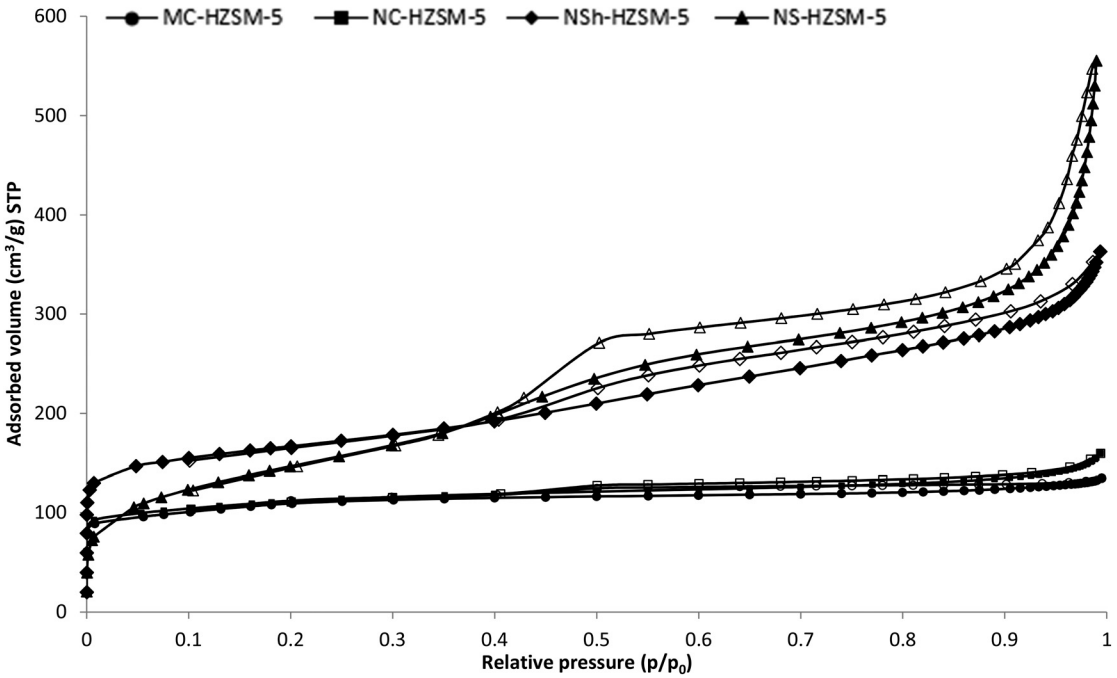

Fig. 4 N_2 adsorption/desorption isotherms at −196 °C of the calcined MC-HZSM-5, NC-HZSM-5, NSh-HZSM-5 and NS-HZSM-5 samples. Full bullets represent adsorption isotherms and empty bullets the desorption ones.

Table 1 Properties of the morphologically different HZSM-5 zeolites

HZSM-5 type	Si/Al ratio[a]	Si/Al of the framework[b]	S_{BET} ($m^2\ g^{-1}$)	$S_{external}$ ($m^2\ g^{-1}$)	Total pore volume ($cm^3\ g^{-1}$)	Micropore volume ($cm^3\ g^{-1}$)	Mesopore volume ($cm^3\ g^{-1}$)	$[PyrH^+]^c$ ($\mu mol\ g^{-1}$)	$[PyrL]^d$ ($\mu mol\ g^{-1}$)
MC-HZSM-5	45	53	395	22	0.167	0.167	—	351	44
NC-HZSM-5	23	29.7	411	34	0.189	0.171	0.018	301	76
NSh-HZSM-5	44	55.4	521	96	0.323	0.189	0.134	103	80
NS-HZSM-5	25	33.4	613	175	0.624	0.273	0.351	218	103

[a] Si/Al molar ratio of the sample determined by XRF. [b] Si/Al molar ratio of the zeolite framework determined from XRF and ^{27}Al MAS NMR. [c] Concentration of pyridine adsorbed on Brønsted acid sites following thermo-desorption at 150 °C. [d] Concentration of pyridine adsorbed on Lewis acid sites following thermo-desorption at 150 °C.

organic structure directing agent C22-6-6 led to the production of lamellar materials for NSh-HZSM-5 (Fig. 2c). The overall thickness of the lamellar stacking of nanosheets was about 20–40 nm. Upon the use of 18-N_3-18 as a surfactant, the increase in the number of quaternary ammonium ions and the length of the carbon chain generated the nanosponge morphology of NS-HZSM-5 (Fig. 2d). The spiky-like nanomaterials are uniform in shape with size varying between 250 and 350 nm.

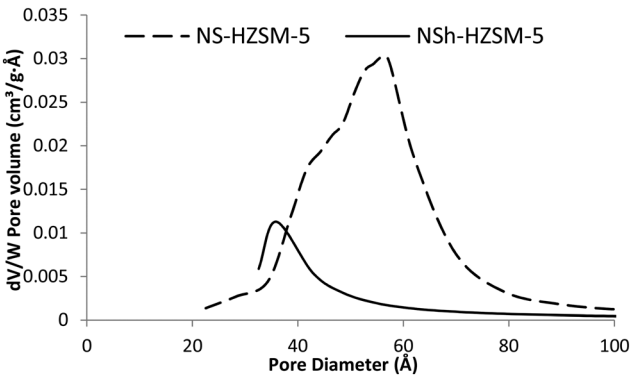

Fig. 5 Mesopore size distribution of the calcined exchanged hierarchical samples NSh-HZSM-5 and NS-HZSM-5.

From the TEM images (Fig. 3a), it is well noticeable that numerous nanosheets of one unit are parallel to each other, presenting an entirely well-ordered assemblage of zeolite nanosheets with a thickness of 2 nm. TEM imaging of NS-HZSM-5 (Fig. 3b) shows interconnected mesopore walls which are composed of zeolite microporous nanocrystals.

3.1.3. Adsorption–desorption of nitrogen. The textural properties of the calcined HZSM-5 with different morphologies were investigated by adsorption–desorption of nitrogen (Fig. 4). MC-HZSM-5 and NC-HZSM-5 displayed both an isotherm of type I as expected for microporous solids. A slight hysteresis was observed for NC-HZSM-5 due to the agglomeration of nanocrystals (interparticle adsorption of N_2). The micropore volumes of MC-HZSM-5 and NC-HZSM-5 were

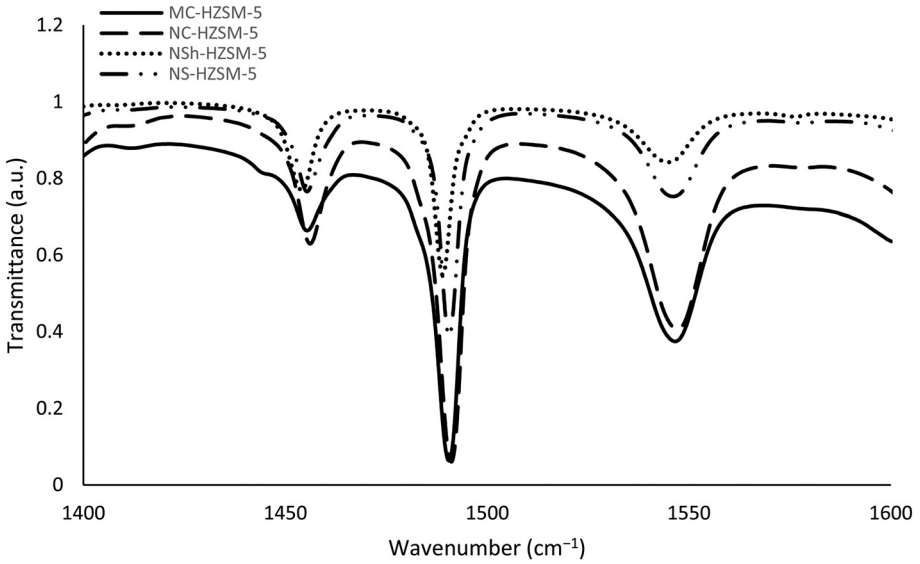

Fig. 6 FTIR spectra after zeolite saturation with pyridine and desorption at 150 °C.

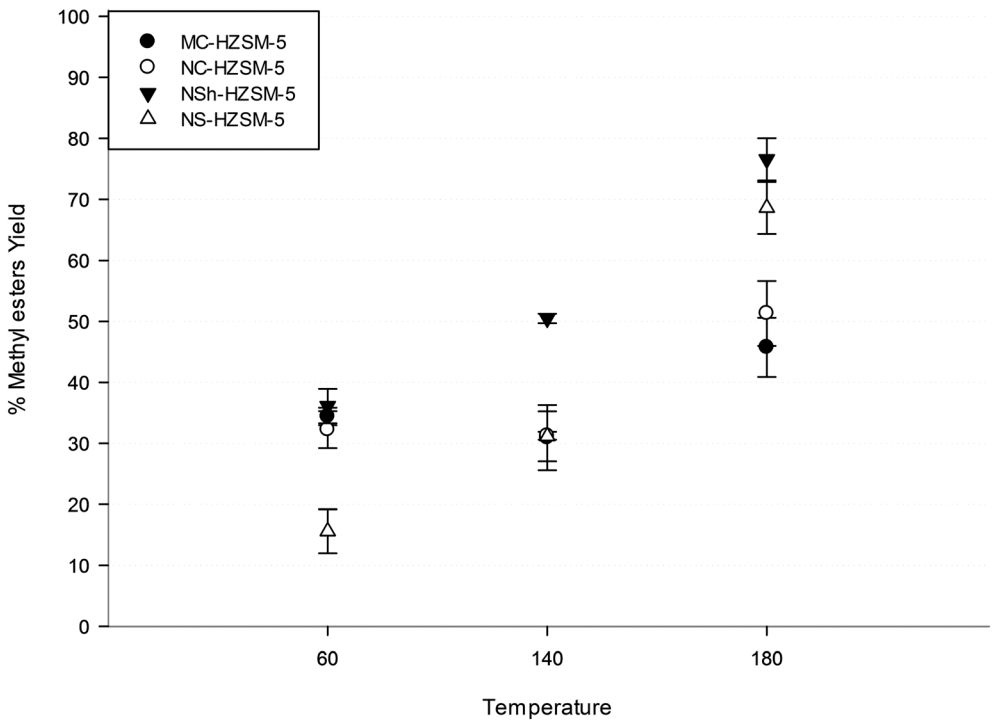

Fig. 7 Reaction temperature variation effect on the esterification of linoleic acid using MC-HZSM-5, NC-HZSM-5, NSh-HZSM-5, and NS-HZSM-5 catalysts at a methanol to linoleic acid molar ratio of 12 : 1, catalyst loading of 10 wt%, stirring rate of 550 rpm, and reaction time of 6 h.

0.167 and 0.171 cm^3 g^{-1}, respectively (Table 1). The adsorption isotherm of NSh-HZSM-5 is of type I at low p/p_0, and of type II with an H4 hysteresis at high p/p_0.[41] The presence of a hysteresis loop in the relative pressure range $0.4 < p/p_0 < 1$ is typical of lamellar materials, due to the stacking of nanosheets. The isotherms of NS-HZSM-5 are of type Ib at low p/p_0 with a micropore volume of 0.273 cm^3 g^{-1} (Table 1). The highest micropore volume relative to the other morphologies of HZSM-5 is explained by the existence of a secondary microporosity due to the presence of the 18-N_3-18 surfactant, in addition to the microporosity induced by the MFI-type lattice. The presence of mesopores on the NS-HZSM-5 zeolite is indicated by the type IV and type II isotherms at $0.4 < p/p_0 < 0.6$ with an H4 hysteresis characteristic of capillary nitrogen gas condensation in the mesopores. At $p/p_0 > 0.9$, interparticle adsorption of N_2 is observed. The mesopore volume of NS-HZSM-5 is estimated to be 0.351 cm^3 g^{-1}. The total pore volume presented in Table 1 increased from MC-HZSM-5 to

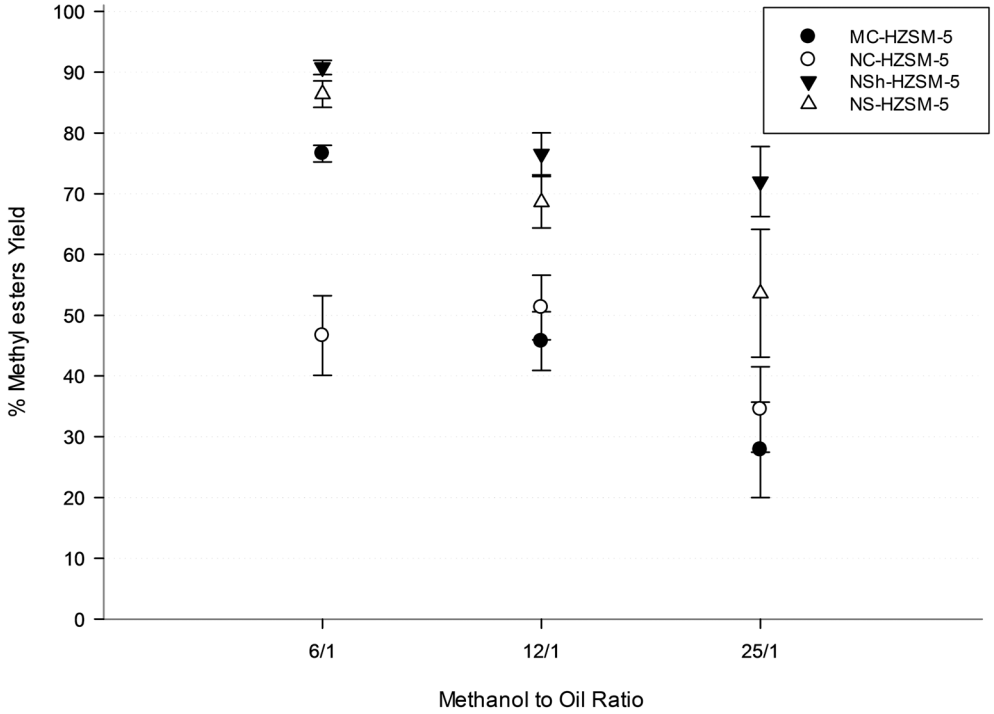

Fig. 8 Effect of methanol to linoleic acid molar ratio variation on the esterification of linoleic acid using MC-HZSM-5, NC-HZSM-5, NSh-HZSM-5, and NS-HZSM-5 catalysts at a catalyst loading of 10 wt%, reaction temperature of 180 °C, stirring rate of 550 rpm and reaction time of 6 h.

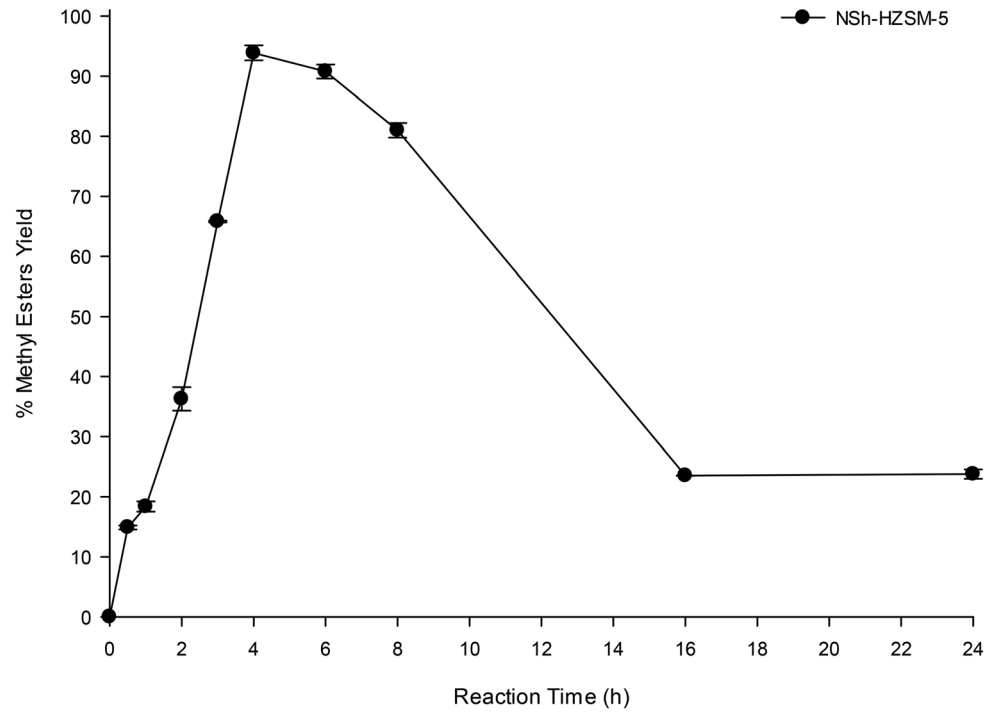

Fig. 9 Effect of reaction time on the esterification of linoleic acid using the NSh-HZSM-5 catalyst at a catalyst loading of 10 wt%, methanol to linoleic acid molar ratio of 6 : 1, reaction temperature of 180 °C, and stirring rate of 550 rpm.

NC-HZSM-5, from NC-HZSM-5 to NSh-HZSM-5 and from NSh-HZSM-5 to NS-HZSM-5, and the BET surface area was higher for the hierarchical materials relative to the microporous zeolites. The BJH pore size distribution of NSh-HZSM-5 was monomodal with a mean mesopore diameter of 35 Å. For NS-HZSM-5 zeolites, the BJH pore size distribution was more intense and quite broad, presenting an average mesopore diameter of 58 Å (Fig. 5). The micropore and mesopore size

Table 2 Thiele modulus variable data for linoleic acid esterification using MC-HZSM-5, NC-HZSM-5, NSh-HZSM-5 and NS-HZSM-5

	MC-HZSM-5	NC-HZSM-5	NSh-HZSM-5	NS-HZSM-5
ε ($cm^3\ g^{-1}$)	0.165	0.166	0.323	0.624
D_{eff} ($m^2\ s^{-1}$)	6.50×10^{-8}	6.52×10^{-8}	1.27×10^{-7}	2.45×10^{-7}
k ($m^2\ h^{-1}$)	0.283	0.213	0.240	0.254
L (m)	0.035×10^{-4}	0.155×10^{-6}	0.010×10^{-6}	0.125×10^{-6}
$\varnothing$	0.437	0.017	0.001	0.008

distributions of all the calcined exchanged samples MC-HZSM-5, NC-HZSM-5, NSh-HZSM-5 and NS-HZSM-5 are presented in section S2 of the ESI.†

3.1.4. FTIR and ^{27}Al MAS NMR. The ^{27}Al solid state MAS NMR spectra of the 4 zeolite samples were recorded. The zeolites exhibit principal resonance at *ca.* 56 ppm corresponding to Al species in tetrahedral coordination present in the MFI framework (section S3 in the ESI†). The ^{27}Al MAS NMR spectra also display a second resonance around 0 ppm attributed to extra framework Al. MC-HZSM-5, NC-HZSM-5, NSh-HZSM-5, and NS-HZSM-5 contain 25%, 15%, 20%, and 30% of extra framework Al, respectively (section S3†). Correspondingly, the Si/Al framework ratios of the different zeolite samples were calculated (Table 1).

The acidity of the morphologically different HZSM-5 catalysts was quantified by FTIR of adsorbed pyridine. Two reasons exist that make pyridine a well-adapted probe molecule for acidity quantification: 1) it can enter the zeolite's internal pores since it has a diameter of 5.6 Å,[42] within the range of the HZSM-5 zeolite pores (5.3–5.6 Å), and 2) it is a strong base with a single electron pair on the nitrogen which forms a pyridinium ion on protonic strong Brønsted sites ($PyrH^+$) found at 1545 cm^{-1} (Fig. 6), and coordinated bonds on weak Lewis acid sites (PyrL) found at 1454 cm^{-1}.[43] Pyridine interacting with both Lewis and Brønsted sites is observed at 1490 cm^{-1} but it does not permit differentiation of the two acid sites and is thus not used to characterize acidity.

The Lewis and Brønsted acid site concentrations were calculated from 1454 cm^{-1} and 1545 cm^{-1} bands, respectively, and the results are reported in Table 1. The Brønsted acidity decreases for hierarchical NSh-HZSM-5 and NS-HSZM-5 with respect to microporous MC-HZSM-5 and NC-HZSM-5 zeolites, whereas the Lewis acidity increases for the bi-porous zeolites relative to the microporous zeolites. Higher catalytic activity is thus expected for the more acidic MC-HZSM-5 and NC-HZSM-5 zeolites. The presence of extra framework Al species can generate Lewis acid sites amounting to the total acidity of the zeolite. However, extra framework Al can be of neutral or cationic nature and therefore does not exclusively account for the Lewis acidic nature of the zeolite,[44] making the correlation between extra framework Al and Lewis acid sites not perfectly linear.[17]

3.2. Optimized reaction conditions of esterification

3.2.1. Effect of reaction temperature on esterification. To assess the reaction temperature effect on the conversion of linoleic acid, experiments using MC-HZSM-5, NC-HZSM-5, NSh-HZSM-5 and NS-HZSM-5 were carried out at three different temperatures of 60, 140 and 180 °C, under the same reaction conditions (stirring rate = 550 rpm, methanol to linoleic acid molar ratio = 12 : 1, catalyst loading = 10 wt%, and reaction time = 6 h). As shown in Fig. 7, the catalytic activity of all the zeolites increased with increasing temperature except for MC-HZSM-5 and NC-HZSM-5 which showed no significant difference in linoleic acid conversion at 60 and 140 °C reaction temperatures with a slightly higher conversion achieved at 60 °C. For all the zeolites, the order of conversion at the optimal reaction temperature of 180 °C was MC-HZSM-5 (45.76%, SD = 4.85) < NC-HZSM-5 (51.31%, SD = 5.33) <

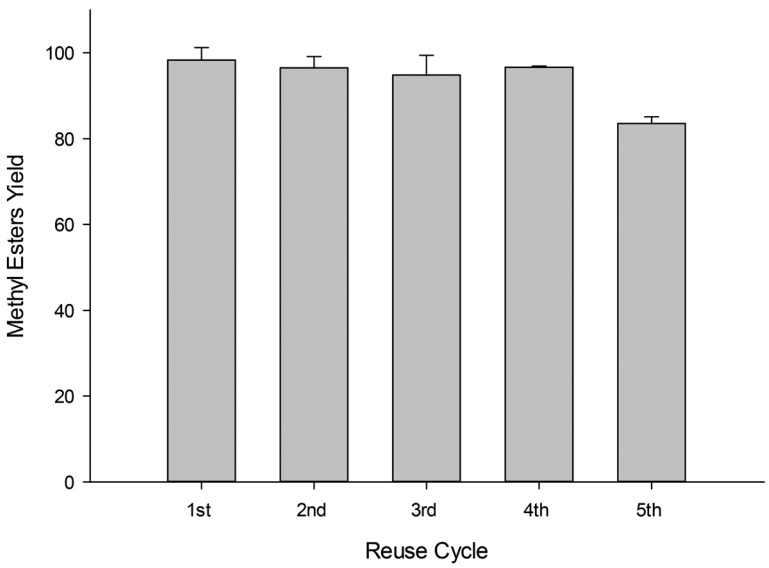

Fig. 10 Methyl ester yield assessment in linoleic acid esterification after NSh-HZSM-5 reuse.

NS-HZSM-5 (68.60%, SD = 3.47) < NSh-HZSM-5 (76.57%, SD = 4.24). When the reaction temperature increases, the reaction rate constant increases according to the Arrhenius equation,[45] and higher conversions are thus achieved. At high reaction temperatures, the average kinetic energy of the molecules present in the reaction increases and causes them to move faster and collide with each other and the catalyst more frequently.[46] However, results show that the increase of acid strength doesn't seem to be the only factor affecting the conversions obtained. The pore size effect on the internal mass transfer limitation appears to play a main role in the esterification of linoleic acid.

3.2.2. Effect of the methanol to linoleic acid ratio on esterification. Since the esterification reaction is reversible, the moles of methanol should be in surplus to direct the reaction towards methyl ester formation.[47] The effect of methanol on the conversion of linoleic acid was evaluated through changing the amount of the alcohol to achieve a methanol/linoleic acid molar ratio of 6 : 1, 12 : 1, and 25 : 1 in the esterification reactions performed with the different catalysts (MC-HZSM-5, NC-HZSM-5, NSh-HZSM-5, and NS-HZSM-5). Similar reaction conditions were used which consisted of 10 wt% catalyst loading, 6 h reaction time, 550 rpm stirring rate, and a fixed optimal temperature of 180 °C. Fig. 8 shows that the linoleic acid conversion rate slightly increased from 46.68% (SD = 6.58) to 51.31%, (SD = 5.33) using NC-HZSM-5 as the molar ratio of methanol to linoleic acid increased from 6 : 1 to 12 : 1, and decreased to 34.50 (SD = 7.01) at the highest alcohol to linoleic acid molar ratio. For all the other catalysts, the conversion rate of linoleic acid decreased as the molar ratio increased from 6 : 1 to 25 : 1. While the equilibrium shift towards the direction of methyl ester formation is a recognized principle when an excess of methanol is adopted in the reaction,[48] at higher methanol to linoleic acid molar ratios, the effect of the reverse reaction is potentially superior to the forward reaction. This phenomenon is due to the slight recombination of methyl esters and water to form linoleic acid. Excess methanol could affect the solubility of the nearly immiscible water and methyl esters encouraging thus the backward reaction to take place.[49] The methanol to linoleic acid molar ratio of 6 : 1 was thus the optimal molar ratio with an order of conversion of NC-HZSM-5 (46.68% SD = 6.58) < MC-HZSM-5 (76.62%, SD = 1.37) < NS-HZSM-5 (86.40%, SD = 2.16) < NSh-HZSM-5 (90.76%, SD = 1.17).

3.2.3. Effect of reaction time on esterification. The effect of reaction time on the conversion of linoleic acid was studied by carrying out experiments using the catalyst which achieved the highest conversion of linoleic acid (hierarchical NSh-HZSM-5) under the optimal reaction conditions (methanol to linoleic acid molar ratio of 6 : 1, catalyst loading of 10%, reaction temperature of 180 °C and stirring rate of 550 rpm). Under these conditions, esterification of linoleic acid was carried out at different reaction times ranging between 0 and 24 h (include times). Fig. 9 displays the effect of reaction time on the converted methyl esters.

According to the results, a reaction time increase from 0.5 to 2 h caused a marked increase in the conversion of linoleic acid from 14.89% (SD = 0.26) to 36.26% (SD = 1.95). An optimal average conversion of 93.87% (SD = 1.25) with a maximum of 95.12% was achieved after 4 h. No further enhancement in the conversion of linoleic acid was observed after 4h of reaction, beyond which a decrease in the methyl ester yield was detected and was significant after 16 h of reaction. Prolonged heating of linoleic acid resulted in its polymerization. A rubber-like deposit which remained insoluble in DCM was found at the bottom of the reactor. Aside from yielding lower linoleic acid conversions, higher reaction times are not favorable for the esterification reactions.

For all experiments, residual linoleic acid was quantified using HPLC. Section S4 in the ESI† presents numeric methyl ester yields and residual linoleic acid under different reaction conditions.

3.2.4. Evaluation of mass transfer limitations of the synthesized catalysts. The effect of external mass transfer limitations was calculated by the Mears criterion. The values indicated that the solid–liquid interface-external mass transfer limitations of all the zeolites were overcome when the stirring speed was 550 rpm (section S5 in the ESI†).

Although the presence of ordered micropores in zeolitic materials enhances their acidity, their sole presence seems to impose intercrystalline diffusion limitations, contributing to the low usage of the zeolite's active volume in the catalyzed esterification reaction.[50] In fact, microporous HZSM-5 zeolites have a small pore size (5.6–5.9 Å) and linoleic acid molecules possess a kinetic diameter of 8.08 Å estimated using eqn (13).[51]

$$\sigma = 1.234 \cdot (M_W)^{1/3} \quad (13)$$

where σ (Å) is the kinetic diameter estimated for hydrocarbons, and M_W is the molecular weight of linoleic acid in g mol^{-1}. This means that it is unlikely for such a molecule to penetrate the pores and reach the active intrinsic sites of the microporous zeolite such as MC-HZSM-5.

Alternative strategies which lead to enhanced accessibility of the active sites within the zeolites for linoleic acid esterification were sought in this study by adopting two different approaches: shortening the diffusion path length of the micropores (NC-HZSM-5) and introducing an additional (meso) porosity to the microporous zeolite crystal (NSh-HZSM-5 and NS-HZSM-5).

For the different morphologies of HZSM-5, the internal mass transfer limitations for the intrinsic diffusion of the oil into the catalyst were evaluated by the estimation of the Thiele modulus ($\varnothing$) (eqn (14)).[52]

$$\varnothing = L \cdot \sqrt{\frac{k}{D_{eff}}} \quad (14)$$

where L (m) represents the characteristic diffusion length of the zeolite defined here as half the crystal size determined by

SEM,[53] k is the reaction rate coefficient (s^{-1}), and D_{eff} is the effective diffusivity of linoleic acid and methanol molecules within the zeolite pores ($m^2\ s^{-1}$).

This method therefore couples the pseudo first-order rate constant k experimental value with the effective diffusion coefficient's theoretical calculation. A value of $\varnothing < 0.1$ indicates that the esterification reaction is free from any diffusion constraints and that the experimental reaction rate is equal to the intrinsic reaction rate.[54]

Eqn (15) was used to calculate the effective diffusion coefficient D_{eff}:[55]

$$D_{eff} = D_{AB} \cdot \frac{\varepsilon}{\tau} \quad (15)$$

where D_{AB} ($m^2\ s^{-1}$) is the molecular diffusion coefficient of solute A (linoleic acid) at low concentration in solvent B (methanol), ε is the porosity of the catalyst, and τ is the zeolite pore tortuosity.

In the present study, the Wilke–Chang method (section S6 in the ESI†) was used to calculate the molecular diffusion coefficient of linoleic acid in methanol, accounting for the reaction temperature of 180 °C.[56] The calculated value was $1.57 \times 10^{-6}\ m^2\ s^{-1}$. The ε for all the zeolites was determined from the nitrogen adsorbed in pore fractions and τ was given a value of 4 as recommended for porous materials.[52]

To generate the reaction rates of the MC-HZSM-5, NC-HZSM-5 and NS-HZSM-5 zeolites, linoleic acid esterification was carried out using a catalyst loading of 10 wt%, methanol to linoleic molar ratio of 6 : 1, reaction temperature of 180 °C, stirring rate of 550 rpm, and reaction time range of 0–4 h. Reaction rate constants of 0.283 $m^2\ h^{-1}$, 0.213 $m^2\ h^{-1}$, 0.240 $m^2\ h^{-1}$, and 0.254 $m^2\ h^{-1}$ were calculated for MC-HZSM-5, NC-HZSM-5, NSh-HZSM-5 and NS-HZSM-5, respectively, in the most linear region (section S7 in the ESI†).

The corresponding D_{eff} values for the zeolites used are listed in Table 2 along with Thiele modulus estimations.

A Thiele modulus value of 0.437 was obtained for micron-sized big crystals MC-HZSM-5, whereas $\varnothing$ = 0.017, 0.008 and 0.001 were estimated for NC-HZSM-5, NS-HZSM-5 and NSh-HZSM-5, respectively. Despite the high Brønsted acid concentration of MC-HZSM-5, the esterification reaction is hindered by mass transfer limitations whereby the zeolite' active volume is not fully available to the linoleic acid molecules. The diffusion properties of MC-HZSM-5 can therefore rationalize its lower catalytic performance at different reaction temperatures, relative to the other hierarchical zeolites. However, despite the weak intrinsic interaction, MC-HZSM-5 still exhibited a catalytic activity of 76.62% (SD = 1.37) which could be attributed to the occurrence of the esterification reaction over the active Brønsted acid sites located at the pore mouths and the external surface of the microporous zeolite crystals.[57] NC-HZSM-5, NSh-HZSM-5 and NS-HZSM-5 had Thiele modulus values of $\varnothing < 0.1$, which prove that the molecular transport effectiveness was enhanced by shortening the diffusion length (NC-HZSM-5) and introducing a secondary mesoporosity (NSh-HZSM-5 and NS-HZSM-5). It is noteworthy that the catalytic performance of NC-HZSM-5 is lower than that of the hierarchical zeolites at the different reaction temperatures and methanol to linoleic acid ratios used. This shows that despite increasing the catalyst effectiveness, a shorter diffusion length is not sufficient to achieve high conversions. In addition to the short diffusion length, generating mesopores that are directly accessible to the linoleic acid molecules from the zeolite crystal's external surface enhanced the molecular transportation to and from the intrinsic active sites of NSh-HZSM-5 and NS-HZSM-5 which showed the highest linoleic acid conversions under optimal esterification reaction conditions.

However, it is noticeable that between the two hierarchical HZSM-5 materials, the NS-HZSM-5 zeolite which possesses a larger mesopore diameter and volume (58 Å and 0.35 $cm^3\ g^{-1}$, respectively, *versus* 35 Å and 0.13 $cm^3\ g^{-1}$ for NSh-HZSM-5) along with a higher number of Brønsted acid sites (218 *versus* 103 μmol g^{-1} for NSh-HZSM-5) exhibited a lower catalytic activity than NS-HZSM-5 (86.40% (SD = 2.16) *versus* 90.76% (SD = 1.17) for NSh-HZSM-5). Turnover frequencies (TOF) (methyl esters produced per Brønsted acid site per specific surface area in one hour) were therefore calculated for the hierarchical zeolites to provide insight into the fundamental factors affecting the catalytic activity of the hierarchical materials. The TOF values were corrected by the BET surface areas found from the nitrogen adsorption/desorption isotherms of the hierarchical zeolites. TOF calculations yielded values of 1.1×10^{-4} and 1.6×10^{-4} $mol_{methyl\ esters}\ \mu mol_{H^+}^{-1}\ m^{-2}\ g\ h^{-1}$ for NSh-HZSM-5 and NS-HZSM-5, respectively. The TOF values of the hierarchical zeolites are closely similar, indicating that the Brønsted acid site concentration of NSh-HZSM-5 and NS-HZSM-5 does not have a significant influence on their catalytic behavior. Introducing mesopores to the microporous zeolite framework is effective for catalytic application if properly located in the crystal. The connectivity between the two types of pores is essential to optimize the efficiency of introducing different levels of porosity in the catalyzed reaction and to satisfy the bulky molecule transfer from the outer mesoporous surface into the intrinsic active framework.[58] Despite the higher Brønsted acid site concentration in NS-HZSM-5, the muddled mesopores induced by surfactant aggregates could have been less effective than the orderly generated mesopores of NSh-HZSM-5 for the selective transport of linoleic acid to the totality of the intrinsic active acid sites, resulting in the NS-HZSM-5 zeolite not operating at its full potential. Consequently, engineering hierarchical zeolites for high catalytic selectivity requires a careful design of mesopores harmoniously located with the micropores. However, such explanation is difficult to be assigned with certitude without added investigation and, so, this will not be considered anymore here.

Besides, the higher Si/Al ratio of NSh-HZSM-5 (Si/Al = 55.4) in comparison with that of NS-HZSM-5 (Si/Al = 33.3) may have led to a higher adsorption capacity of linoleic acid onto the active surface of the zeolite. In fact, the more hydrophobic the zeolite is, the more its acidic properties decrease.

However, it also avoids the adsorption of the water by-product which will induce its deactivation by blocking the access of the fatty acid.[59] It appears that water was more easily adsorbed onto the surface of the more hydrophilic NS-HZSM-5, hindering the linoleic acid molecules to react with the acid sites and thus, yielding lower conversions despite its higher acidity. The same phenomenon might have occurred with the more hydrophilic NC-HZSM-5 zeolite (Si/Al = 29.7) which displayed a poor catalytic activity in spite of its higher concentration of Brønsted acid sites. It is also worth highlighting that this more hydrophilic character of NC-HZSM-5 is responsible for the difference in the performance of the catalysts with a methanol to linoleic acid molar ratio of 12 : 1, whereby the order of conversion was MC-HZSM-5 < NC-HZSM-5 < NS-HZSM-5 < NSh-HZSM-5, and a molar ratio of 6 : 1, whereby the order of linoleic acid conversion was NC-HZSM-5 < MC-HZSM-5 < NS-HZSM-5 < NSh-HZSM-5. The reaction with a methanol to linoleic acid ratio of 6 : 1 is lower in methanol concentration than the one with a molar ratio of 12 : 1. This means that there is less methanol for the same amount of linoleic acid. And with few methanol molecules, the competition with water for the adsorption sites was more brutal leaving less space for the already lower concentration of methanol in comparison with the reaction happening at a molar ratio of 12 : 1, thus leading to the faster deactivation of NC-HZSM-5. Moreover, although the mass transfer is more limited in MC-HZSM-5, the catalyst's higher hydrophobic character (Si/Al = 53) permitted the rapid desorption of the produced water during the esterification reaction and allowed linoleic acid and methanol to react more efficiently over the acid sites on the external surface or in the pore mouth regions of the microporous zeolite. In terms of diffusion limitations, reactant selectivity, and relative hydrophobicity, NSh-HZSM-5 offered the best catalytic performance in modelling biodiesel production.

3.2.5. Catalyst regeneration. The reusability of the NSh-HZSM-5 catalyst was assessed by performing five successive 4 h linoleic acid esterification cycles using 10 g of linoleic acid, under the optimum defined reaction conditions (6 : 1 methanol to linoleic acid ratio, 180 °C reaction temperature, 6 h reaction time, and 10% catalyst loading). At the end of each cycle, the used catalyst was separated from the liquid phase by filtration and heated at 105 °C. The liquid phase (methanol, DCM and methyl esters) product mixture yield was around 95% for the first 4 cycles and decreased to 83.56% (SD = 1.28) after the 5th cycle (Fig. 10). This shows that the NSh-HZSM-5 catalyst retains its catalytic activity after 4 consecutive cycles before linoleic acid conversion drops substantially.

4. Conclusion

Esterification of linoleic acid with methanol was successfully catalyzed using hierarchical HZSM-5 zeolite catalysts produced in nanosheet and nanosponge morphologies as compared to highly acidic conventional big and nano-crystals of HZSM-5 zeolites. Improved accessibility and molecular transport of linoleic acid from the outer mesoporous surface to the intrinsic active zeolitic framework resulted in achieving high conversions of 86.40% (SD = 2.16) for NS-HZSM-5 and 90.76% (SD = 1.17) for NSh-HZSM-5 under similar reaction conditions. A maximum linoleic acid conversion of 95.12% was reached for the esterification of linoleic acid using NSh-HZSM-5 at 4 h reaction time, 10 wt% catalyst loading, 6 : 1 methanol to linoleic acid molar ratio and 180 °C and maintained for 4 consecutive cycles, after which the conversion value dropped to 83.56%. Although highly accessible and acidic, HZSM-5 nanosponges did not operate at their full potential as compared to HZSM-5 nanosheets given their higher hydrophilicity which favored water adsorption onto their surface, and due to the connectivity between the different levels of porosity (micro and meso-porosity) which wasn't optimal for effective selective transport of linoleic acid and methyl ester molecules to and from the intrinsic active sites of the catalyst.

Conflicts of interest

There are no conflicts to declare.

Acknowledgements

This research was supported by the University Research Board (URB) at the American University of Beirut, Lebanon.

References

1 A. Demirbas, *Biodiesel production from vegetable oils by supercritical methanol*, 2005.
2 G. Baskar and R. Aiswarya, Trends in catalytic production of biodiesel from various feedstocks, *Renewable Sustainable Energy Rev.*, 2016, **57**, 496–504, Available from: http://linkinghub.elsevier.com/retrieve/pii/S1364032115014847.
3 M. Tubino, J. G. R. Junior and G. F. Bauerfeldt, Biodiesel synthesis with alkaline catalysts: A new refractometric monitoring and kinetic study, *Fuel*, 2014, **125**, 164–172, Available from: http://linkinghub.elsevier.com/retrieve/pii/S001623611400115X.
4 Y. H. Tan, M. O. Abdullah and C. Nolasco-Hipolito, The potential of waste cooking oil-based biodiesel using heterogeneous catalyst derived from various calcined eggshells coupled with an emulsification technique: A review on the emission reduction and engine performance, *Renewable Sustainable Energy Rev.*, 2015, **47**, 589–603, Available from: http://linkinghub.elsevier.com/retrieve/pii/S1364032115002014.
5 M. Atapour and H.-R. Kariminia, Characterization and transesterification of Iranian bitter almond oil for biodiesel production, *Appl. Energy*, 2011, **88**(7), 2377–2381, Available from: http://linkinghub.elsevier.com/retrieve/pii/S0306261911000171.
6 B. E. H. P. Freedman, E. H. Pryde and T. L. Mounts, Variables affecting the yields of fatty esters from

transesterified vegetable oils, *J. Am. Oil Chem. Soc.*, 1984, **60**(10), 1638–1643.

7 K. H. Chung, D. R. Chang and B. G. Park, Removal of free fatty acid in waste frying oil by esterification with methanol on zeolite catalysts, *Bioresour. Technol.*, 2008, **99**(16), 7438–7443.

8 Y. Fan, X. Lin, G. Shi, H. Liu and X. Bao, Realumination of dealuminated HZSM-5 zeolite by citric acid treatment and its application in preparing FCC gasoline hydro-upgrading catalyst, *Microporous Mesoporous Mater.*, 2007, **98**(1–3), 174–181, Available from: http://linkinghub.elsevier.com/retrieve/pii/S1387181106003295.

9 I. Batonneau-gener, A. Yonli, S. Hazael-Pascal, J. Pedro Marques, J. Madeira Lopes and M. Guisnet, *et al.*, Influence of steaming and acid-leaching treatments on the hydrophobicity of HBEA zeolite determined under static conditions, *Microporous Mesoporous Mater.*, 2008, **110**(2–3), 480–487, Available from: http://linkinghub.elsevier.com/retrieve/pii/S1387181107003976.

10 K. Saravanan, B. Tyagi, R. S. Shukla and H. C. Bajaj, Esterification of palmitic acid with methanol over template-assisted mesoporous sulfated zirconia solid acid catalyst, *Appl. Catal., B*, 2015, **172–173**, 108–115, Available from: http://linkinghub.elsevier.com/retrieve/pii/S092633731500065X.

11 M. Zabeti, W. M. A. Wan Daud and M. K. Aroua, Activity of solid catalysts for biodiesel production: A review, *Fuel Process. Technol.*, 2009, **90**(6), 770–777, Available from: http://linkinghub.elsevier.com/retrieve/pii/S0378382009000629.

12 Z. Helwani, M. R. Othman, N. Aziz, J. Kim and W. J. N. Fernando, Solid heterogeneous catalysts for transesterification of triglycerides with methanol: A review, *Appl. Catal., A*, 2009, **363**(1–2), 1–10, Available from: http://linkinghub.elsevier.com/retrieve/pii/S0926860X09003652.

13 S. M. Auerbach, K. A. Carrado and P. K. Dutta, *Handbook of zeolite science and technology*, CRC press, 2003.

14 A. Astafan, Y. Pouilloux, J. Patarin, N. Bats, C. Bouchy and T. Jean Daou, *et al.*, Impact of extreme downsizing of *BEA-type zeolite crystals on n-hexadecane hydroisomerization, *New J. Chem.*, 2016, **40**(5), 4335–4343, Available from: http://xlink.rsc.org/?DOI=C5NJ02837J.

15 A. Astafan, M. A. Benghalem, Y. Pouilloux, J. Patarin, N. Bats and C. Bouchy, *et al.*, Particular properties of the coke formed on nano-sponge *BEA zeolite during ethanol-to-hydrocarbons transformation, *J. Catal.*, 2016, **336**, 1–10, Available from: https://linkinghub.elsevier.com/retrieve/pii/S0021951716000087.

16 P. Losch, J. F. Kolb, A. Astafan, T. J. Daou, L. Pinard and P. Pale, *et al.*, Eco-compatible zeolite-catalysed continuous halogenation of aromatics, *Green Chem.*, 2016, **18**(17), 4714–4724, Available from: http://xlink.rsc.org/?DOI=C6GC00731G.

17 C. Miranda, J. Urresta, H. Cruchade, A. Tran, M. Benghalem and A. Astafan, *et al.*, Exploring the impact of zeolite porous voids in liquid phase reactions: The case of glycerol etherification by tert-butyl alcohol, *J. Catal.*, 2018, **365**, 249–260, Available from: https://linkinghub.elsevier.com/retrieve/pii/S0021951718302628.

18 S. S. Vieira, Z. M. Magriotis, I. Graça, A. Fernandes, M. F. Ribeiro and J. M. F. M. Lopes, *et al.*, Production of biodiesel using HZSM-5 zeolites modified with citric acid and SO_4^{2-}/La_2O_3, *Catal. Today*, 2017, **279**, 267–273.

19 N. Narkhede and A. Patel, Efficient synthesis of biodiesel over a recyclable catalyst comprising a monolacunary silicotungstate and zeolite Hβ, *RSC Adv.*, 2014, **4**(110), 64379–64387.

20 O. Mowla, E. Kennedy and M. Stockenhuber, In-situ FTIR study on the mechanism of both steps of zeolite-catalysed hydroesterification reaction in the context of biodiesel manufacturing, *Fuel*, 2018, **232**, 12–26, Available from: https://doi.org/10.1016/j.fuel.2018.05.096.

21 S. O. Otieno, C. O. Kowenje, A. Okoyo, D. M. Onyango, K. O. Amisi and K. M. Nzioka, ScienceDirect Optimizing production of biodiesel catalysed by chemically tuned natural zeolites, *Mater. Today: Proc.*, 2018, **5**(4), 10561–10569, Available from: https://doi.org/10.1016/j.matpr.2017.12.388.

22 D. N. Thoai, S. Photaworn, A. Kumar, K. Prasertsit and C. Tongurai, A Novel Chemical Method for Determining Ester Content in Biodiesel, *Energy Procedia*, 2017, **138**, 536–543, Available from: http://linkinghub.elsevier.com/retrieve/pii/S1876610217350993.

23 A. M. Doyle, Z. T. Alismaeel, T. M. Albayati and A. S. Abbas, High purity FAU-type zeolite catalysts from shale rock for biodiesel production, *Fuel*, 2017, **199**, 394–402, Available from: http://dx.doi.org/10.1016/j.fuel.2017.02.098.

24 K. V. Thiruvengadaravi, J. Nandagopal, P. Baskaralingam, V. Sathya Selva Bala and S. Sivanesan, Acid-catalyzed esterification of karanja (Pongamia pinnata) oil with high free fatty acids for biodiesel production, *Fuel*, 2012, **98**, 1–4, Available from: http://linkinghub.elsevier.com/retrieve/pii/S0016236112001706.

25 Y.-M. Park, S.-H. Chung, H. J. Eom, J.-S. Lee and K.-Y. Lee, Tungsten oxide zirconia as solid superacid catalyst for esterification of waste acid oil (dark oil), *Bioresour. Technol.*, 2010, **101**(17), 6589–6593, Available from: http://linkinghub.elsevier.com/retrieve/pii/S0960852410005869.

26 K. Ramachandran, P. Sivakumar, T. Suganya and S. Renganathan, Production of biodiesel from mixed waste vegetable oil using an aluminium hydrogen sulphate as a heterogeneous acid catalyst, *Bioresour. Technol.*, 2011, **102**(15), 7289–7293, Available from: http://linkinghub.elsevier.com/retrieve/pii/S0960852411006390.

27 J. Gardy, A. Hassanpour, X. Lai, M. H. Ahmed and M. Rehan, Biodiesel production from used cooking oil using a novel surface functionalised TiO_2 nano-catalyst, *Appl. Catal., B*, 2017, **207**, 297–310, Available from: http://linkinghub.elsevier.com/retrieve/pii/S0926337317300978.

28 J. Jin, X. Zhang, Y. Li, H. Li, W. Wu and Y. Cui, *et al.*, A Simple Route to Synthesize Mesoporous ZSM-5 Templated by Ammonium-Modified Chitosan, *Chem. – Eur. J.*,

2012, **18**(51), 16549–16555, Available from: http://doi.wiley.com/10.1002/chem.201201614.

29 K. Y. Nandiwale, N. D. Galande, S. A. Raut and V. V. Bokade, Benzylation of acetic acid to benzyl acetate over highly active and reusable Micro/Meso-HZSM-5, *Chem. Eng. Res. Des.*, 2015, **93**, 584–590, Available from: https://linkinghub.elsevier.com/retrieve/pii/S0263876214002792.

30 K. Sun, J. Lu, L. Ma, Y. Han, Z. Fu and J. Ding, A comparative study on the catalytic performance of different types of zeolites for biodiesel production, *Fuel*, 2015, **158**, 848–854, Available from: http://dx.doi.org/10.1016/j.fuel.2015.06.048.

31 K. Na, M. Choi, W. Park, Y. Sakamoto, O. Terasaki and R. Ryoo, Pillared MFI Zeolite Nanosheets of a Single-Unit-Cell Thickness, *J. Am. Chem. Soc.*, 2010, **132**(12), 4169–4177, Available from: http://pubs.acs.org/doi/abs/10.1021/ja908382n.

32 K. Na, C. Jo, J. Kim, K. Cho, J. Jung and Y. Seo, *et al.*, Directing Zeolite Structures into Hierarchically Nanoporous Architectures, *Science*, 2011, **333**(6040), 328–332, Available from: http://www.sciencemag.org/lookup/doi/10.1126/science.1204452.

33 J. Dhainaut, T. J. Daou, Y. Bidal, N. Bats, B. Harbuzaru and G. Lapisardi, *et al.*, One-pot structural conversion of magadiite into MFI zeolite nanosheets using mononitrogen surfactants as structure and shape-directing agents, *CrystEngComm*, 2013, **15**(15), 3009, Available from: http://xlink.rsc.org/?DOI=c3ce40118a.

34 M. Guisnet, P. Ayrault and J. Datka, Acid properties of dealuminated mordenites studied by IR spectroscopy. 2. Concentration, acid strength and heterogeneity of OH groups, *Pol. J. Chem.*, 1997, **71**(10), 1455–1461.

35 D. Massiot, F. Fayon, M. Capron, I. King, S. Le Calvé and B. Alonso, *et al.*, Modelling one- and two-dimensional solid-state NMR spectra, *Magn. Reson. Chem.*, 2002, **40**(1), 70–76, Available from: http://doi.wiley.com/10.1002/mrc.984.

36 A. Gratzfeld-Husgen and R. Schuster, *HPLC for food analysis*, Agil Technol., 2001, p. 136.

37 A. S. Abbas, T. M. Albayati, Z. T. Alismaeel and A. M. Doyle, Kinetics and Mass Transfer Study of Oleic Acid Esterification over Prepared Nanoporous HY zeolite, *Iraqi J. Chem. Pet. Eng.*, 2016, **17**(1), 47–60.

38 T. De Roo, J. Wieme, G. J. Heynderickx and G. B. Marin, Estimation of intrinsic rate coefficients in vinyl chloride suspension polymerization, *Polymer*, 2005, **46**(19), 8340–8354, Available from: https://linkinghub.elsevier.com/retrieve/pii/S0032386105008967.

39 T. H. Dang, B. H. Chen and D. J. Lee, Application of kaolin-based catalysts in biodiesel production via trans-esterification of vegetable oils in excess methanol, *Bioresour. Technol.*, 2013, **145**, 175–181, Available from: http://dx.doi.org/10.1016/j.biortech.2012.12.024.

40 A. Birla, B. Singh, S. N. Upadhyay and Y. C. Sharma, Kinetics studies of synthesis of biodiesel from waste frying oil using a heterogeneous catalyst derived from snail shell, *Bioresour. Technol.*, 2012, **106**, 95–100, Available from: http://linkinghub.elsevier.com/retrieve/pii/S0960852411016762.

41 I. Kabalan, B. Lebeau, H. Nouali, J. Toufaily, T. Hamieh and B. Koubaissy, *et al.*, New Generation of Zeolite Materials for Environmental Applications, *J. Phys. Chem. C*, 2016, **120**(5), 2688–2697, Available from: http://pubs.acs.org/doi/10.1021/acs.jpcc.5b10052.

42 P. Bräuer, P. L. Ng, O. Situmorang, I. Hitchcock and C. D'Agostino, Effect of Al content on number and location of hydroxyl acid species in zeolites: a DRIFTS quantitative protocol without the need for molar extinction coefficients, *RSC Adv.*, 2017, **7**(83), 52604–52613, Available from: http://xlink.rsc.org/?DOI=C7RA10699H.

43 E. G. Derouane, J. C. Védrine, R. R. Pinto, P. M. Borges, L. Costa and M. A. N. D. A. Lemos, *et al.*, The Acidity of Zeolites: Concepts, Measurements and Relation to Catalysis: A Review on Experimental and Theoretical Methods for the Study of Zeolite Acidity, *Catal. Rev.: Sci. Eng.*, 2013, **55**(4), 454–515, Available from: http://www.tandfonline.com/doi/abs/10.1080/01614940.2013.822266.

44 R. D. Shannon, K. H. Gardner, R. H. Staley, G. Bergeret, P. Gallezot and A. Auroux, The nature of the nonframework aluminum species formed during the dehydroxylation of H-Y, *J. Phys. Chem.*, 1985, **89**(22), 4778–4788.

45 K. J. Laidler, The development of the Arrhenius equation, *J. Chem. Educ.*, 1984, **61**(6), 494, Available from: http://pubs.acs.org/doi/abs/10.1021/ed061p494.

46 P. D. Pacey, Changing conceptions of activation energy, *J. Chem. Educ.*, 1981, **58**(8), 612, Available from: http://pubs.acs.org/doi/abs/10.1021/ed058p612.

47 F. Qiu, Y. Li, D. Yang, X. Li and P. Sun, Heterogeneous solid base nanocatalyst: Preparation, characterization and application in biodiesel production, *Bioresour. Technol.*, 2011, **102**(5), 4150–4156, Available from: http://linkinghub.elsevier.com/retrieve/pii/S0960852410020341.

48 W. Xie and L. Zhao, Heterogeneous CaO–MoO_3–SBA-15 catalysts for biodiesel production from soybean oil, *Energy Convers. Manage.*, 2014, **79**, 34–42, Available from: http://linkinghub.elsevier.com/retrieve/pii/S0196890413007620.

49 Q. Shu, B. Yang, H. Yuan, S. Qing and G. Zhu, Synthesis of biodiesel from soybean oil and methanol catalyzed by zeolite beta modified with La^{3+}, *Catal. Commun.*, 2007, **8**(12), 2159–2165.

50 A. Taguchi and F. Schüth, Ordered mesoporous materials in catalysis, *Microporous Mesoporous Mater.*, 2005, **77**(1), 1–45, Available from: http://linkinghub.elsevier.com/retrieve/pii/S1387181104003038.

51 H. WANG and M. FRENKLACH, Transport properties of polycyclic aromatic hydrocarbons for flame modeling, *Combust. Flame*, 1994, **96**(1–2), 163–170, Available from: http://linkinghub.elsevier.com/retrieve/pii/0010218094901678.

52 J. J. Carberry, *Chemical and catalytic reaction engineering*, Cour Corp., 2001.

53 O. Levenspiel, Chemical Reaction Engineering, *Ind. Eng. Chem. Res.*, 1999, **38**(11), 4140–4143, Available from: http://pubs.acs.org/doi/abs/10.1021/ie990488g.

54 M. Boltz, P. Losch, B. Louis, G. Rioland, L. Tzanis and T. J. Daou, MFI-type zeolite nanosheets for gas-phase aromatics

chlorination: a strategy to overcome mass transfer limitations, *RSC Adv.*, 2014, **4**(52), 27242–27249, Available from: http://xlink.rsc.org/?DOI=C4RA02747G.

55 B. E. Poling, J. M. Prausnitz and J. P. O'connell, *The properties of gases and liquids*, New York Mcgraw-Hill, 2001, p. 5.

56 C. R. Wilke and P. Chang, *AICHE J.*, 1955, **1**, 264.

57 W. J. Roth, B. Gil, W. Makowski, B. Marszalek and P. Eliášová, Layer like porous materials with hierarchical structure, *Chem. Soc. Rev.*, 2016, **45**(12), 3400–3438, Available from: http://xlink.rsc.org/?DOI=C5CS00508F.

58 J. Pérez-Ramírez, C. H. Christensen, K. Egeblad, C. H. Christensen and J. C. Groen, Hierarchical zeolites: enhanced utilisation of microporous crystals in catalysis by advances in materials design, *Chem. Soc. Rev.*, 2008, **37**(11), 2530, Available from: http://xlink.rsc.org/?DOI=b809030k.

59 A. A. Kiss, A. C. Dimian and G. Rothenberg, Solid Acid Catalysts for Biodiesel Production -Towards Sustainable Energy, *Adv. Synth. Catal.*, 2006, **348**(1–2), 75–81, Available from: http://doi.wiley.com/10.1002/adsc.200505160.